GE-International Journal of Engineering Research
Vol. 5, Issue 1, January 2017 Impact Factor- 5.613
ISSN(O): 2321-1717, ISSN(P): 2394-420X

Website: www.aarf.asia Email : editor@aarf.asia , editoraarf@gmail.com

DISTINGUISHABILITY-TO-NOISE RATIO (DNR), A PARAMETER TO DETERMINE THE DISCRIMINATING CAPABILITY OF AN EIT INSTRUMENT

S. Talha Ahsan[1,2] and H. McCann[1,3]
[1]*School* of Electrical and Electronic Engineering, University of Manchester, UK
[2]Dept. of Electrical Engineering, Usman Institute of Technology (UIT), Karachi, Pakistan.
[3]School of Engineering, University of Edinburgh, UK.

ABSTRACT

An important aspect of an EIT (Electrical Impedance Tomography) instrument's performance is its Distinguishability, i.e. effectiveness in discriminating the conductivity contrasts present in the object being probed, in the presence of measurement noise. A comparison of the value of distinguishability with that of measurement noise is critical, as good detection capability due to high distinguishability can be masked by the large noise present in the EIT instrument. This paper suggests a newly-coined term distinguishability-to-noise ratio (DNR), which is the value of distinguishability divided by that of measurement noise. It is proposed that DNR which quantifies the comparison of distinguishability with the measurement noise, would be useful in determining the capability of an EIT system to detect conductivity contrasts. For the EIT instrument fEITER (functional EIT of Evoked Responses), measured values of distinguishability and DNR have been presented, and the reconstructed images have been analyzed in this context, showing that the lower is DNR, the higher is the error in the size of an inserted inhomogeneity as shown in the reconstructed image.

Key Words: Distinguishability, Noise, Detection, Image, SNR, DNR

1. INTRODUCTION TO DISTINGUISHABILITY

1.1 Definitions

The distinguishability of an EIT instrument has many possible definitions. [1] talks about an inhomogeneous conductivity distribution being *distinguishable* from a homogeneous conductivity distribution and suggests the term distinguishability, pointing out its similarity to another term, visibility, used by [2]. [3] defines distinguishability as the "ability of a pattern of currents to distinguish between two conductivities". Distinguishability is thus synonymous with discrimination – an important characteristic of any measurement system [4]. Distinguishability is generally defined in literature as the change in the boundary voltage levels, caused by the change in the conductivity distribution of the subject [5, 6]. Conductivity changes must themselves be defined in terms of both conductivity contrast and spatial extent (figure 2 in [7]).

Mathematically, distinguishability has been defined as the norm of the voltage differences (resulting from the conditions of pre- and post-change in conductivity distribution within the subject) divided by the norm of the applied current [1, 8]. In this definition, the numerator is a number which represents the change in voltages, pre- and post-perturbation, measured on all of the electrode-pairs for all of the current patterns. There can be many ways to calculate this number [3, 9]. One possible way to calculate a number representing the change in voltages can be to

use either the mean or median of the voltage measurements normalised by the value of the injected current. Equations 1 and 2 enable calculation of distinguishability (δ), as the mean of ΔV_i, which are the absolute differences of the normalised voltages.

$$\Delta V_i = \left| V_{i,pre} - V_{i,post} \right| \quad (1)$$

$$\delta = \frac{1}{N} \sum_{i=1}^{N} \Delta V_i \quad (2)$$

where:

$V_{i,pre}$ and $V_{i,post}$ are the pre- and post-perturbation values, respectively, of the ith voltage measurement, normalised by the current, and

i is called the measurement index having values from 1 to N, where N is the total number of voltage measurements for all combinations of measurement-electrode-pairs and current injection patterns, comprising one frame of data.

The unit of distinguishability (δ) is either ohm, or volts normalised for the value of the injected current. The latter unit has been followed in this paper. Equations 1 and 2 have been used for the analysis of results.

1.2 Factors controlling Distinguishability

Distinguishability of an EIT system depends upon the cumulative effect of following several factors:

a) number of current sources [10, 11, 12]

b) type of current drives [13] and current patterns [14, 9, 15, 16]

c) number, size and configuration of the electrodes [17, 18, 19, 20, 21]

d) measurement precision of the system [6, 7]

The above factors can be collectively called ‘measurement configuration’. These have been discussed in detail in the above-cited sources and need not be repeated here.

2. DISTINGUISHABILITY-TO-NOISE RATIO (DNR)

In the context of EIT systems’ performance, the comparative relationship between distinguishability and measurement noise is critical, as good detection capability of the EIT instrument due to high distinguishability can be masked by the measurement noise. One approach incorporates noise into the definition of distinguishability, proposing that distinguishability is a product of the impedance change amplitude, the measurement strategy and the inverse of the noise amplitude [22]. This approach has been used to explore different current stimulation patterns. [23] have suggested various parameters to evaluate and compare EIT systems’ performance. These parameters characterize noise and accuracy in measured data and reconstructed image, as well as detectability and distinguishability of single and multiple contrasts. [24] have proposed a new noise performance metric for EIT algorithms which is based on distinguishability.

In order to quantify the comparative link between distinguishability and measurement noise considered separately, in case of a given set of current injection and voltage measurement strategies, a scheme is hereby proposed. The value of distinguishability calculated as per equation 2, is divided by the measurement noise (calculated as standard deviation in the voltage measurements), resulting in a non-dimensional quantity normalised for a certain value of current. This quantity is hereby called distinguishability-to-noise ratio (DNR). It is proposed that DNR which quantifies the comparison of distinguishability with the measurement noise, would be useful in determining the capability of an EIT system to detect conductivity contrasts, as supported by the results discussed later.

The impact of the measurement signal-to-noise ratio (SNR) on the quality of the reconstructed image is well-established [19, 25]. In order to have good spatial resolution in images, it is necessary to have both high distinguish-

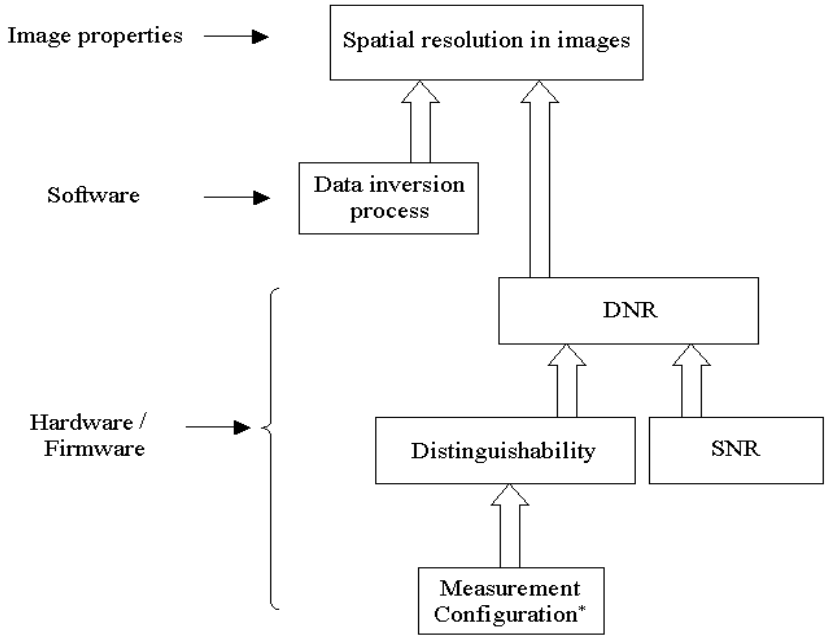

Fig. 1 Inter-dependence among SNR, DNR and Image quality in an EIT system

* *Number of current sources; type of current drives; number, size & configuration of electrodes; and system precision*

ability and low measurement noise; this would mean high value of the proposed parameter DNR in the EIT instrument. This is a necessary but not sufficient condition, as the other factor controlling image quality is the image reconstruction process itself. The overall link among SNR, distinguishability, DNR and spatial resolution in images can be depicted schematically as in figure 1.

Distinguishability is not uniform throughout the subject, due to the nature of the electric field resulting from the injected current in an EIT system. It is always poorer in the centre of the subject, compared with peripheral regions where the electrodes are placed [26]. Therefore, having high DNR near the centre of the subject is a major challenge for EIT instruments.

Next section presents the distinghuishability and DNR results measured for the 35-channel bio-medical EIT instrument fEITER (functional Electrical Impedance Tomography of Evoked Responses) built at the University of Manchester [27]. The aim of the fEITER system is to achieve brain function imaging at sub-second time-scales, with the measurement sensitivity of around 80 dB at the high data-capturing rate of 100 frames/sec. Firmware loaded on a Xilinx Virtex-4 SX35 FPGA performs the EIT operation, with injection current of 10 kHz frequency and 1 mA peak-to-peak amplitude. Images are reconstructed with the method employed in [28], using the EIDORS 3D software.

3. RESULTS OF MEASURED DISTINGUISHABILITY AND DNR

In order to assess the noise- and distinguishability-related performance of the bio-medical EIT instrument fEITER, tank tests were performed. Measured voltage results of these tank tests were reported in [29]. In these tests, the typical measured value of SNR was around 80 dB. Test results using precision resistor wheel were reported in [27].

Following is a presentation of the tank test results in terms of the measured values of distinguishability and DNR, and an analysis of the reconstructed images. Similar work has been reported in literature for other EIT instruments, e.g. [8, 5, 30].

3.1 Test Methodology

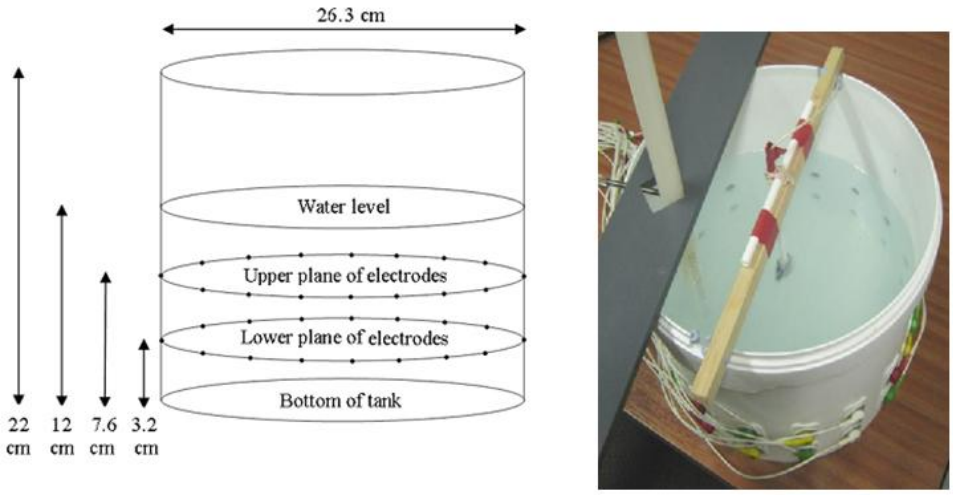

Fig. 2 (a) 3D view of cylindrical tank (b) Nylon rod inserted in tank

The cylindrical tank (figure 2) had the diameter and height of, respectively, 26.3 and 22 cm, and the water depth during tank tests was 12 cm. On the inner surface of the tank, 32 electrodes were arranged in two planes of 16. Electrodes 1 to 16 made up the lower plane, at a height of 3.2 cm from the bottom of the tank. Electrodes 17 to 32 made up the upper plane, at a height of 7.6 cm from the bottom of the tank. The reference electrode was dipped into the water at the centre position of the tank, from a wooden bar fixed at the top of the tank. For the tests, the tank was pre-filled with homogeneous medium (almost 7 litres of saline solution of typical conductivity 500 µS/cm), through which planar, polar current injection patterns were passed, and inhomogeneities were introduced during EIT data capture. There were 8 current injection patterns per plane, *viz.* 1-9, 2-10, 3-11, 4-12, 5-13, 6-14, 7-15, 8-16 in the lower plane and 17-25, 18-26, 19-27, 20-28, 21-29, 22-30, 23-31, 24-32 in the upper plane (figure 3).

For the test, initially a nylon rod having length more than the water depth and diameter of 2.1 cm was used as the single solid inhomogeneity. EIT data capture using fEITER system was started. After approximately 30 seconds, the nylon rod was slowly inserted into the tank at a position in front of electrodes 10 and 26 and kept there till the end of the one minute data capture. The rod was fully inside the water and it barely touched the bottom. Because of the clamp,

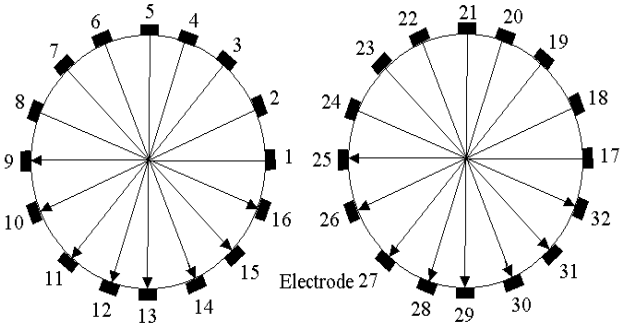

Fig. 3 Top view of current injection patterns for the normalised electrodes in lower (left figure) and upper planes

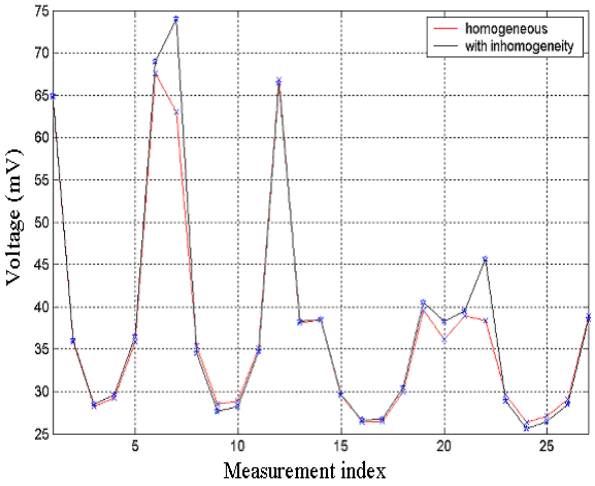

Fig. 4 Pre- and post-perturbation peak-to-peak magnitudes, averaged over 500 frames for the current injection pattern 1-9 only

it was perfectly stable (figure 2(b)).

For the analysis of the measured voltage data, in both pre- and post-perturbation cases, the average of ith voltage measurement was calculated over 500 frames, where i is the measurement index i.e. combination of current-injection- and voltage measurement-pairs, ranging from 1 to 420.

3.2 Distinguishability and DNR of the EIT instrument for solid inhomogeneity

Figure 4 shows the plots of measured voltages for pre-perturbation i.e. homogeneous (red colour) and post-perturbation (grey colour) cases, for a sub-set of the measurement indices (numbers 1 to 27, involving all the voltage measurements for the current injection at electrode-pair 1-9). ΔV_i (as per equation 1) is the absolute difference in the two normalised voltage magnitudes of pre- and post-perturbation cases and, for the first 27 measurement indices, is visible as the difference between the two plots in figure 4.

Figure 5(a) shows the plot of ΔV_i for all 420 measurement indices. Figure 5(b) shows two example time-based plots over one minute, of the normalised voltage magnitudes, for two of the measurement indices from figure 5(a). These plots are for measurement index number 7 (red in both (a) and (b)) and 218 (black in both (a) and (b)). These measurement indices correspond to, respectively, '1-9 (current injection-pair) 10-11 (measurement-pair)' and '17-25, 8-9'. Table 1 shows the five largest values of absolute changes in normalised voltage magnitudes along with their corresponding current-injection and measurement electrode-pairs.

Distinguishability can be calculated (as per equation 2) as the average of ΔV_i calculated over all 420 values of measurement index i. The Distinguishability of the fEITER system for this inhomogeneity, i.e. nylon rod of cross-sectional area 0.64 % of the tank, at this position, comes out to be 963.2 μV as normalised for 1 mA injected current. The pre- and post-perturbation mean standard deviations (calculated over 500 frames in each case) are, respectively, 10.26 μV and 12.38 μV. Using the higher value of 12.38 μV as denominator, with the distinguishability of 963.2 μV as numerator, gives the worst case DNR value as 77.8. (Figure 9 in section 3.4 shows the image reconstructed for this case.)

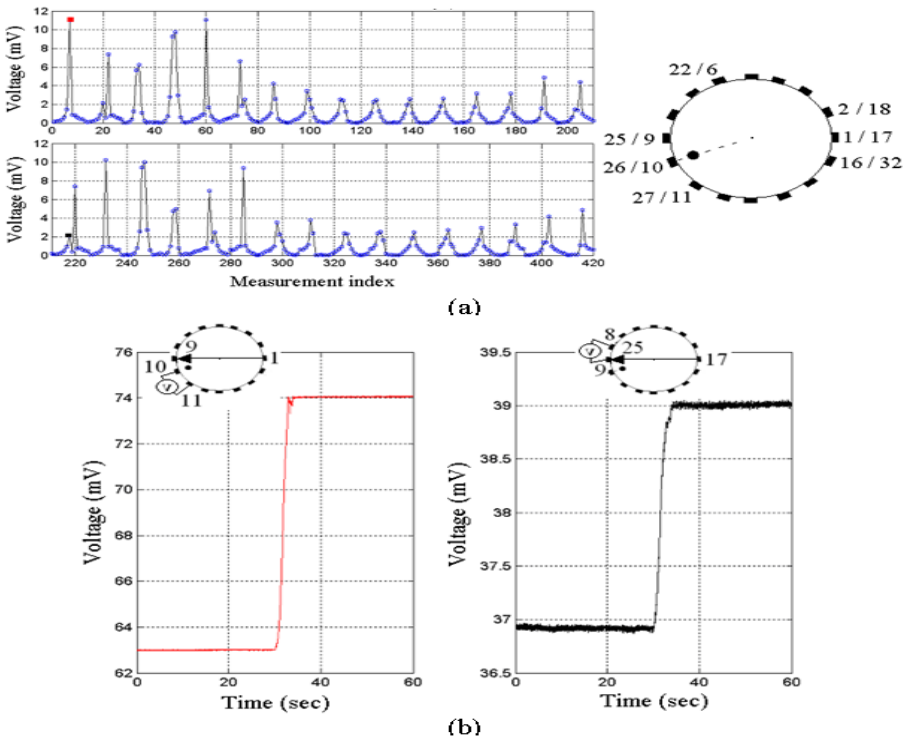

Fig. 5 (a) Absolute change in normalised magnitudes, pre- and post-insertion of nylon rod in tank (b) Time-based plots of normalised magnitudes for two measurement indices of (a) i.e. numbers 7 ('1-9, 10-11'; red plot) and 218 ('17-25, 8-9'; black plot)

S. No.	Measur-ement index	'current injection-pair, voltage-measurement-pair'	ΔV_i (mV)
1	60	'3-11, 9-10'	11.07
2	7	'1-9, 10-11'	11.05
3	232	'17-25, 26-27'	10.23
4	247	'18-26, 10-11'	10.02
	48	'2-10, 26-27'	9.75

Table 1. Five largest absolute changes in inserted normalised voltage magnitudes, pre- and post-insertion of nylon rod in tank

S. No.	In-homogeneity	Cross-sectional area (% of tank)	Distingu-ishability (μV)	DNR
1	Wooden rod	0.036	42.4	3.78
2	Nylon rod	0.64	963.2	77.8
3	PEEK rod	1.39	1678.4	94.3
4	No in-homogeneity (reference solution)	-	6.7	0.62

Table 2. Distinguishability measured for different objects in tank at the same position

Tank tests, with the same methodology were conducted with two other solid inhomogeneities, *viz.* wooden and PEEK rods, each inserted (one at a time) at the same position as shown in figure 5(a). The results are presented in table 2. These results convey a comparative picture of the distinguishability of fEITER for the inhomogeneities of different material as well as spatial size, introduced in the subject at the same location. An important aspect of these results is the almost linear relationship between spatial size of the introduced inhomogeneity and the resulting distinguishability. The last result in table 2 shows the instrument's distinguishability measured for a homogeneous solution. It gives a very low value, though the value being non-zero suggests that the solution was not ideally homogeneous. Section 3.4 presents conductivity images reconstructed using these results, for wooden, PEEK and nylon rods.

3.3 'Detectable' and 'Undetectable' Distinguishability, for a solid inhomogeneity of small spatial size

The results of measured distinguishability for wooden rod in table 2 present a special case of the inhomogeneity of very small spatial extent (occupying only 0.036 % of the area of the subject), though of high conductivity contrast. Figure 6(a) shows the plot of ΔV_i (calculated using equation 1) for all 420 measurement indices, in this case. Figure 6(b) shows time-based plots over one minute, of the normalised voltage magnitudes, for two of the measurement indices from figure 6(a), having medium-to-low values of voltage change. These plots are for measurement index number 165 (red in both (a) and (b)) and 166 (black in both (a) and (b)). These measurement indices correspond to, respectively, '7-15 (current injection-pair) 10-11 (measurement-pair)' and '7-15, 11-12'. The red and black plots show a voltage magnitude change of, respectively, 116 μV and 44.9 μV. The black plot shows that it is nearing the noise limit, with the measured change in voltage magnitude (44.9 μV) slightly higher than the noise level. The black plot still shows a well-resolved change of 0.162 %. This is the typical case of having voltage change bordering on 'detectability' limit. Smaller voltage changes would be merged into noise voltage and would not be detectable.

The overall situation is depicted by the low distinguishability value of 42.4 μV, which is expected to be bordering

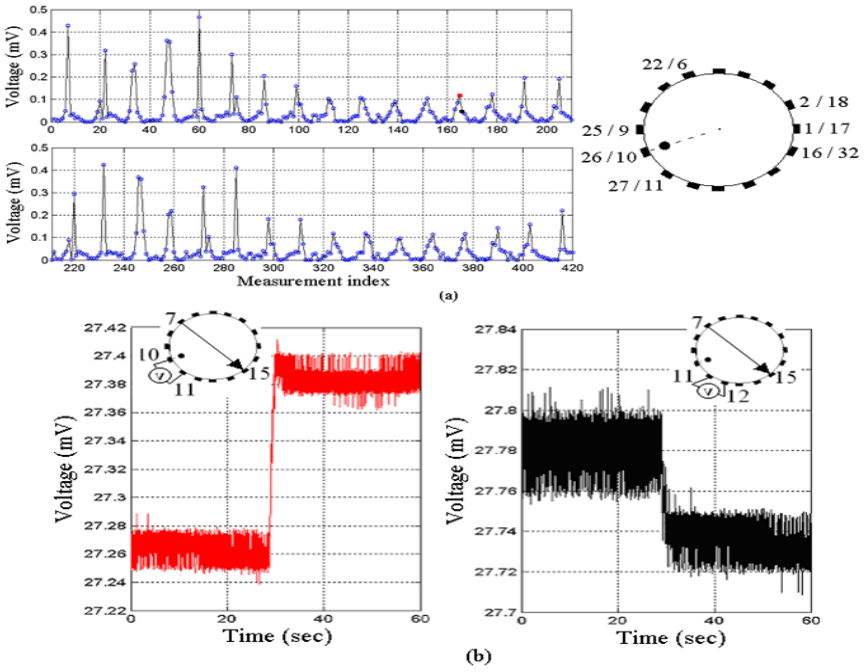

Fig. 6 (a) Absolute change in normalised magnitudes, pre- and post-insertion of wooden rod in tank
(b) Time-based plots of normalised magnitudes, for two measurement indices of (a)
i.e. numbers 165 ('7-15, 10-11'; red plot) and 166 ('7-15, 11-12'; black plot)

on ‘detectability limit’. The pre- and post-perturbation mean standard deviations (calculated over 500 frames in each case) are, respectively, 11.22 μV and 10.55 μV. Using the higher of the two as denominator and the distinguishability of 42.4 μV as numerator gives DNR value as 3.78. Comparing with the case of nylon rod at the same position (when DNR was 77.8), this DNR value is almost 20 times less, which is due to the much smaller-sized inhomogeneity. (Figure 8 presents the image reconstructed for this case.)

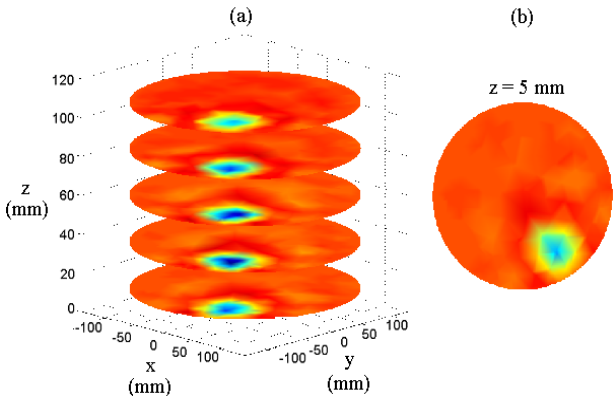

Fig. 7 Difference image of conductivity when a PEEK rod was inserted near the tank periphery in front of electrode 10, showing (a) slices at multiple planes (b) top view of the plane at z=5 mm planes

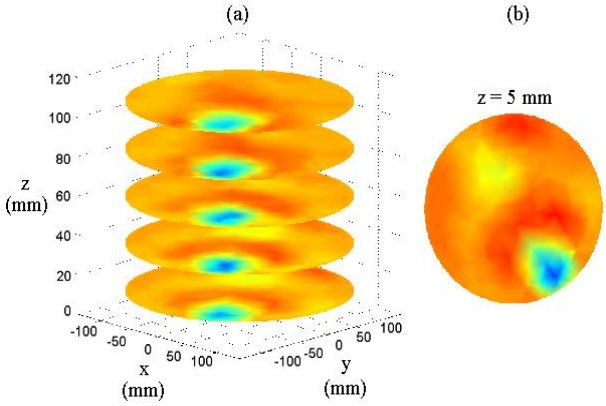

Fig. 8 Difference image of conductivity when a Wooden rod was inserted near the tank periphery in front of electrode 10, showing (a) slices at multiple planes (b) top view of the plane at z=5 mm

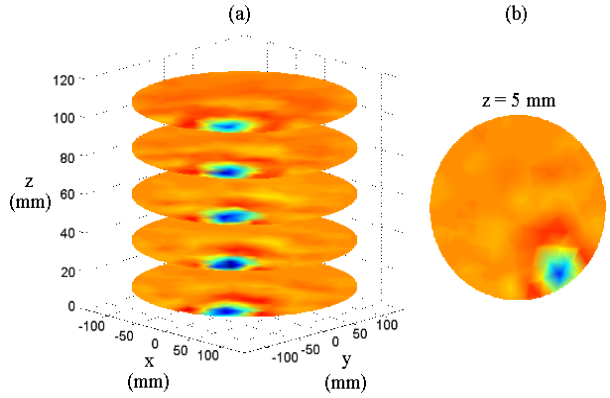

Fig. 9 Difference image of conductivity when a Nylon rod was inserted near the tank periphery in front of electrode 10, showing (a) slices at multiple planes (b) top view of the plane at z=5 mm planes

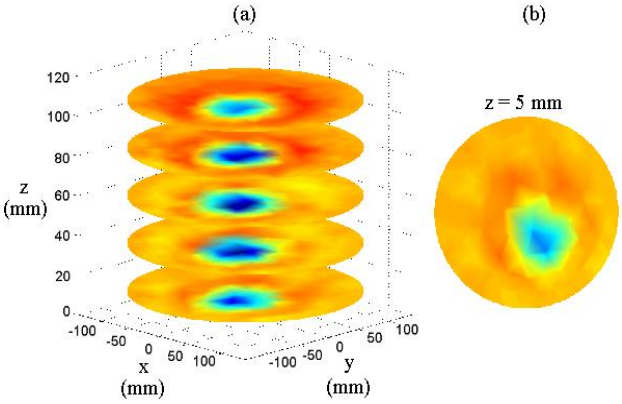

Fig. 10 Difference image of conductivity when a Nylon rod was inserted near the tank centre, on the line joining tank centre with electrode 10, showing (a) slices at multiple planes (b) top view of the plane at z=5 mm

3.4 Reconstructed images and link with DNR values

For the tank test data presented in table 2 for the inhomogeneities of wooden, nylon and PEEK rods, images were reconstructed. Another image for one more data set was reconstructed, when the same nylon rod was inserted near the tank centre, on the line joining electrode 10 and the centre of the tank.

Image reconstruction was performed using the method employed in [28]. It is based on General Tikhonov Regularization, with a model of 4413 tetrahedral elements and uses EIDORS 3D software. Reconstruction uses the real component of the captured data (normalized to 1 mA current). 100 data frames in the homogeneous part of data capture are averaged to give a 'reference frame'. The images are reconstructed from the differences in voltage measurements between the 'reference frame' and the 'target frame' at t=50 s (based on a 5 frame average).

Figures 7, 8, 9 and 10 show the solutions for the four cases mentioned above, plotted in ranges corresponding to their own local maxima and minima. Part (b) of these figures show a scalar cut plane plot for each solution at the tank height of z =5 mm. All reconstructed images are consistent with the inhomogeneity being almost in line of electrode 10 (x=100, y=-100).

Figure 7 is the image reconstructed for the PEEK rod, having the distinguishability of 1678.4 µV and DNR of 94.3. The ratio of actual diameters of tank to PEEK rod ('actual dia.-ratio') is 8.5:1, whereas the image shows a dia.-ratio of 6.33:1 (for blurred green portion). Thus in the image, this inhomogeneity is shown with a size slightly larger than the actual, with an error of 25.5 % (s. no. 1 in table 3).

Figure 8 is the image reconstructed for the wooden rod, having the distinguishability of 42.4 µV and DNR of 3.78. The two 'actual dia.-ratio' and 'image dia.-ratio' (for green portion) in this case are, respectively, 52.6:1 and 4.22:1. The huge difference in the two ratios, reflecting 92 % error (s. no. 2 in table 3), can be related to two factors: i) Very low value of DNR and ii) larger size of the tetrahedral element (viz-a-viz the size of inhomogeneity) used in data inversion. Thus, as shown in figure 1, both of DNR and data inversion process are affecting the image quality in this case.

Figure 9 is the image reconstructed for the nylon rod, having the distinguishability of 963.2 µV and DNR of 77.8. The two 'actual dia.-ratio' and 'image dia.-ratio' (for green portion) in this case are, respectively, 12.5:1 and 4.75:1. The difference in the two ratios, reflecting 62 % error (s. no. 3 in table 3), is worse than the case of PEEK rod which

S. No.	In-homogeneity	Distinguishability (µV)	DNR	Tank-to-rod Diameter-ratio		
				Actual	In the reconstructed image	Error (%)
1	PEEK rod	1678.4	94.3	8.5	6.33	25.5
2	Wooden rod	42.4	3.78	52.6	4.22	92
3	Nylon rod	963.2	77.8	12.5	4.75	62
4	Nylon rod (inserted in tank-centre)	380.6	32.45	12.5	3.2	74.4

Table 3. DNR and the 'tank-to-rod diameter-ratios' measured as actual vs in the reconstructed images

had the largest values of distinguishability and DNR. However, it is better than the case of wooden rod which had the smallest values of distinguishability and DNR.

Thus, the comparative data of these images viz-a-viz DNR values, given in table 3, show that as DNR decreases (s. no. 1, 3, 4 and 2 in this order), the size of the portion of the image showing inhomogeneity increases erroneously. These images are showing the *location* of the inserted inhomogeneity correctly, even in the case of the smallest size of wooden rod. However, the *size* of the shown inhomogeneity is in error (i.e. the difference between the tank-to-rod diameter-ratio as in actual vs that in the reconstructed image), with the error being smallest and largest in the case of, respectively, largest and smallest distinguishability and DNR.

It is further interesting to compare figures 9 and 10, which are showing the same object (nylon rod) inserted near, respectively, periphery and centre of the tank. The distinguishability and DNR values for the latter case were, respectively, 380.6 μV and 32.45. The 'actual dia.-ratio' in this case was the same as that for the case of figure 9 i.e. 12.5:1. However, figure 10 has 'image dia.-ratio' (green portion) of 3.2:1, having an error of 74.4 % (s. no. 4 in table 3). Thus, as distinguishability and DNR decrease towards the tank centre, size of the green portion showing inhomogeneity has more error in figure 10, as compared with figure 9.

4. CONCLUSION

The comparison of distinguishability of an EIT instrument with the measurement noise determines its capability to discriminate the conductivity contrasts. In order to characterize this comparative link, a new term distinguishability-to-noise ratio (DNR) has been proposed in this paper, which is the distinguishability value divided by the noise in the voltage measurements. The result is a non-dimensional quantity, normalised for the value of the injected current. Usefulness of DNR in determining the capability of an EIT system to detect conductivity contrasts has been demonstrated through the examples of the inserted solid inhomogeneities. Results show that the lower is DNR, the higher is the error in the size of the inserted inhomogeneity as shown in the reconstructed image.

ACKNOWLEDGEMENTS

Author S. Talha Ahsan gratefully acknowledges Dr. J. L. Davidson (University of Manchester) for performing the reconstruction of images and Dr. P. Wright (University of Manchester) for providing the fEITER hardware system he had designed.

ABBREVIATIONS USED

DNR: Distinguishability-to-noise ratio; EIT: Electrical impedance tomography; fEITER: Functional Electrical Impedance Tomography of Evoked Responses; FPGA: Field Programmable Gate Array; PEEK: Polyether Ether Ketone; SNR: Signal-to-noise ratio.

REFERENCES

1. Isaacson D 1986 Distinguishability of conductivities by electric current computed tomography IEEE Tr. Med. Imaging **5** 91-5

2. Seagar A D, T S Yeo and R H T Bates 1984 Full-wave computed tomography Part 2: Resolution limits *IEE Proc. Science* **131** Pt. A 616-22

3. Gisser D G, D Isaacson and J C Newell 1987 Current topics in impedance imaging *Clin. Phys. Physiol. Meas.* **8** *suppl. A* 39-46

4. Sydenham P H, N H Hancock and R Thorn 1989 *Introduction to Measurement Science and Engineering* John Wiley and Sons

5. Fuks L F, M Cheney, D Isaacson, D G Gisser and J C Newell 1991 Detection and imaging of electric conductivity and permittivity at low frequency *IEEE Tr. Biomed. Eng.* **38** 1106-10

6. Kao T-J, J C Newell, G J Saulnier and D Isaacson 2003 Distinguishability of inhomogeneities using planar electrode arrays and different patterns of applied excitation *Physiol. Meas.* **24** 403-11

7. Halter R J, A Hartov and K D Paulsen, 2008 Video rate electrical impedance tomography of vascular changes: preclinical development *Physiol. Meas.* **29** 349-64

8. Newell J C, D G Gisser and D Isaacson 1988 An electric current tomograph IEEE Tr. Biomed. Eng. **35** 828-33

9. Cheney M and D Isaacson 1992 Distinguishability in impedance imaging IEEE Tr. Biomed. Eng. **39** 852-60

10. Saulnier G J, R S Blue, J C Newell, D Isaacson and P M Edic 2001 Electrical impedance tomography *IEEE Signal Processing Magazine Nov 2001* 31-43

11. Saulnier G J, A S Ross and N Liu 2006 A high-precision voltage source for EIT *Physiol. Meas.* **27** S221-S236

12. Ashe J, D Shoudy, G Boverman, J Sabatini, T Kao and B Amm 2014 A high precision parallel current drive experimental EIT system, *15th Conf. Biomed. EIT Canada*

13. Shi X, X Dong, W Shuai, F You, F Fu and R Liu 2006 Pseudo-polar drive patterns for brain electrical impedance tomography *Physiol. Meas.* **27** 1071-80

14. Gisser D G, D Isaacson and J C Newell 1988 Theory and performance of an adaptive current tomography system *Clin. Phys. Physiol. Meas.* **9** *suppl. A* 35-41

15. Demidenko E, A Hartov, N Soni and K D Paulsen 2005 On optimal current patterns for electrical impedance tomography *IEEE Trans. Biomed. Eng.* **52** 238-48

16. Silva O L, R G Lima, T C Martins, F S de Moura, R S Tavares and M S G Tsuzuki 2016 Influence of current injection pattern and electric potential measurement strategies in electrical impedance tomography *Control Engineering Practice (Elsevier online)*

17. Dickin F J and M Wang 1995 Impedance sensors – conducting systems, chapter 5 in *Process Tomography: Principles, Techniques and Applications* Williams R A and Beck M S ed. by (UK: Butterworth Heinemann)

18. Pinheiro P A T, W W Loh and F J Dickin 1998 Optimal sized electrodes for electrical resistance tomography *Electronics Letters* **34** 69-70

19. Polydorides N and H McCann 2002 Electrode configurations for improved spatial resolution in electrical impedance tomography *Meas. Sci. Technol.* **13** 1862-70

20. Mamatjan Y, B Grychtol and A Adler 2014 Effective electrode positions and stimulation patterns for head EIT *Proc. 15th Conf. Biomed. EIT, Canada* 85

21. Farooq A, J N Tehrani, A L McEwan 2014 Improvements and artifact analysis in conductivity images using multiple internal electrodes *Physiol. Meas.* **15** 2263-74

22. Adler A, P Gaggero and Y Maimaitijiang 2010 Distinguishability in EIT using a hypothesis-testing model, *J. Phys.: Conf. Ser.* **224** 012056

23. Yasin M, S Bohm, P O Gaggero and A Adler 2011 Evaluation of EIT system performance *Physiol. Meas.* **32,** 851

24. Adler A, F Braun and J Sola 2015 Distinguishability as a noise performance metric for EIT algorithms, *16th Conf. Biomed. EIT Switzerland*

25. Stephenson D R, T A York and R Mann 2007 Performance and requirements of process ERT instruments *Proc. 5th World Congress on IPT Bergen Norway* 895-901

26. Seagar A D, D C Barber and B H Brown 1987 Theoretical limits to sensitivity and resolution in impedance imaging *Clin. Phys. Physiol. Meas*. **8** *Suppl. A* 13-31

27. McCann H, S T Ahsan, J L Davidson, R L Robinson, P Wright and C J D Pomfrett 2011 A portable instrument for high-speed brain function imaging: fEITER, *Proc.33rd IEEE EMBS Conf.* 7029-32

28. Davidson J L, L S Ruffino, D R Stephenson, R Mann, B D Grieve and T A York 2004 Three-dimensional electrical impedance tomography applied to a metal-walled filtration test platform *Meas. Sci. Technol.* **15** 2263-74

29. Davidson J L, P Wright, S T Ahsan, R Robinson, C J D Pomfrett and H McCann 2009 fEITER - a New biomedical EIT instrument for OR and ICU applications *10th Conf. Biomed. EIT, Univ. of Manchester UK*

30. Lee K H, Y T Kim, T I Oh and E J Woo 2007 Complex conductivity spectra of seven materials and phantom design for EIT *Proc. ICEBI'07 Graz Austria* 344-7